

Micro-scale modelling of bovine cortical bone fracture: Analysis of crack propagation and microstructure using X-FEM

Adel A. Abdel-Wahab, Angelo R. Maligno, and Vadim V. Silberschmidt

Wolfson School of Mechanical and Manufacturing Engineering, Loughborough University, Loughborough, Leicestershire, LE11 3TU, UK

Abstract

Bone fracture susceptibility increased by factors such as bone loss, microstructure changes, and material properties variations. Therefore, investigation of the microstructure and material properties effect on the crack propagation and the global response at macro-scale level is of great importance. A non-uniform distribution of osteons in a cortical bone tissue results in a localization of deformation processes. Such localization can affect bone performance under external load and initiate fracture or assist its propagation. Once the fracture initiates, that distribution can play an important role on the crack propagation process at micro-scale level. Subsequently, the global response at macro-scale level could also be affected. In this study, a two-dimensional numerical (finite-element) fracture model for osteonal bovine cortical bone was developed with account for its microstructure using X-FEM. The topology of a transverse-radial cross section of a bovine cortical bone was captured with optical microscopy. The mechanical properties for the microstructural features of the cross-section were obtained with a use of the nanoindentation technique. Both the topology and nanoindentation data were used as input to the model formulated with the Abaqus 6.10 finite-element software. The area, directly reflecting micro-scale information, was embedded into the region with homogenised properties of the cortical bone. The simulations provide the macro-scale global response, crack propagation paths and the distribution of maximum principal stress fields at the micro-scale level for three different microscopic topologies; homogeneous, two phase composite model and threr phase composite model under tensile loading condition.

The calculated stress fields for various cases of topologies demonstrate different patterns due to implementation of microstructural features in the finite-element model. There is an important role of the microstructure on the crack propagation trajectory. The suggested approach emphasizes the importance of microstructural features, especially cement lines, in development of bone failure.

Keywords: finite-element, X-FEM, fracture, microcrack, bovine cortical bone, nanoindentation.

1. Introduction

Bone fracture is a health difficulty with intense economic and social consequences. To plan a prevention therapies and treatment strategies a scientific knowledge of

bone fracture mechanisms is profound [1]. The mechanical behaviour of the failure process of cortical bone tissue is affected by several factors, such as, bone mineral density (bone loss), microstructure changes, variations in its material properties and accumulation of microcracks [2, 3]. Factors such as porosity, mineralization, collagen fibre orientation, diameter and spacing and other aspects of histological structure strongly affect mechanical properties; have positive effect on crack initiation and negative influence on their growth [4]. The effect of bone quantity on the mechanical behaviour and structural integrity of bone was established previously [5, 6], however, more in-depth investigations are still required of the contributory effects of microstructure, material properties, and microcrack propagation [3, 7]. These can be characterized as bone quality measures; an improved understanding of bone quality, particularly, resistance to crack initiation and propagation can help in accessing bone fracture risk [8]. It is well known that damage occurs in both trabecular and cortical bone due to daily activity loading regime [9]. Microdamage can be repaired by remodelling process, however, if the bone's repair mechanism is deficient, fragility fractures may result due to minor trauma, especially for ageing bone [10]. Experimentally, both damage location and morphology in the form of linear microcracks were characterised [11-13]. Also, the relationship between the crack length and propagation in compact bone tested in cyclic fatigue under four-point bending was investigated [10]. It was found in this sense that if linear microcracks possess enough energy or the repairing system is deficient; it can propagate and lead to fracture.

Bone is a complex hierarchical composite. Histologically, bovine cortical bone is characterised as primary and secondary. During bone growth, primary bone is established on existing bone surfaces, such as circumferential lamellar bone underneath the periosteal surface [10]. Blood vessels are surrounded by concentric lamellae known as primary osteons. Primary osteons are smaller, shorter, have few number and no cement lines as compared to compact bone's secondary osteons [14]. Secondary osteons in compact bone result from absorption and replacement of old bone by new lamellar bone through remodelling process. They are round to ellipsoidal shapes in radial-transverse sections of cortical bones and form the basic building blocks of the cortical bone tissue [10]. Their diameters vary between 100-400 μm and can be between 1-2 mm in length [15]. Each osteon comprises several lamellae surrounding central Haversian canal and bounded by cement line that separates one osteon from another and the surrounding interstitial bone. The material properties of the thin amorphous interface – cement line – are not fully established yet [16]. Secondary compact bone can be considered as composite material [2, 7]. In such a composite model, osteons are represents as the fibres and interstitial bone as the matrix. A cement line is a weak interface separates osteons from interstitial bone.

Few finite element models have been developed to investigate the effect of microstructure constituents on the deformation and fracture behaviour of cortical bone tissue. Prendergast *et al.* [16] modelled numerically an osteon to investigate the relationship between damage formation and local strain to ascertain that

microdamage changes the local strain fields in the bone microstructure. Dong *et al.* [17] used a generalized self-consistent method to estimate the effective elastic moduli of a fiber-reinforced composite, and the model was considered useful to examine the dependence of the elastic properties of cortical bone on its porosity. In another study, Budyn *et al.* [18] introduced a multiple scale method for modelling multiple crack growth in cortical bone tissue under tension using X-FEM. In another attempt a micro-finite element model of osteonal cortical bone tissue to evaluate the interaction between the osteons and microcracks was developed by Raeisi Najafi *et al.* [19]. The effect of the cement lines on the microcrack propagation paths and on the macroscale behaviour as well as relating it to a homogenised material and a composite model containing no cement lines of osteonal cortical bone tissue can promote our understanding of their role to inhibit bone fracture. In this perspective, a 2D microstructural finite-element model to investigate the effect of microstructure constituents, particularly cement lines, on microcrack propagation paths and global macroscopic behaviour is presented. This study was dedicated to the failure process of a microstructural osteonal cell of cortical bone tissue using eXtended Finite Element Method (XFEM) implemented into Abaqus 6.10. To investigate the effect of the microstructural constituents on both the failure process and the global response three different models were developed: homogeneous material model, three phase composite model with cement lines, and two phase composite model without cement lines, see Fig. 1.

2. Materials and Methods

2.1 Model Geometry

A microstructural cell of secondary osteonal cortical bone is modelled as: homogeneous, two phase composite and three-phase composite model. At microstructural scale three different constituents are characterized: osteons, interstitial bone, and cement lines. Osteons are considered as fibres since they are approximately circular, interstitial bone is considered a matrix as it fills the gaps between the osteons. Each osteon is surrounded by a thin layer – cement lines – see Fig. 1c. In the two phase composite model without cement lines; interstitial bone constitutive model was assigned to the cement line regions resulting in a two phase material model. Several light microscopy images for a radial-transverse section of the bovine cortical bone were captured from medial position; a sample picture is shown in **Fig. 1a**. Those images were used to measure the geometrical parameters of Haversian system: osteons diameters, Haversian canal diameters, cement line thicknesses and diameters of voids. All the images have identical dimensions of 0.7 mm × 0.525 mm (width × height). The statistical analysis for those images exhibited an osteons volumetric fraction of approx. 60% and a porosity ratio between 1.6% and 5.3%. The average width of the cement lines was between 1- 5 μm . The area, directly reflecting micro-scale information, was embedded into the region with homogenised properties of the cortical bone making the dimensions of the model 0.9 mm × 0.725 mm × 0.3 mm (width × height × thickness). This homogenised area

enabled the application of uniform deformation and reaction forces at both the cell sides. All the parameters were measured from those images using digital image analysis software, Image-Pro Express [20]. The observations obtained from that analysis were statistically analysed to be fitted to one of the well known distributions that describe the random phenomena. It was found that the random distribution of the osteons diameters can be fitted with the hypersecant distribution curve described by the continuous scale and location parameter values of 35.3 and 99.9, respectively. On the other hand, Dagum (4P) curve revealed a good fit for the Haversian canal diameters and can be defined by $k=1.52$, $\alpha=2.7$, $\beta=12.9$, and $\gamma=3.3$. The average diameters of osteon fibre and Haversian canal were $99.89 \mu\text{m}$ and $23.1 \mu\text{m}$, respectively. The random microstructure of the model, Fig. 1c, was established using Matlab [21]. Using a script written by the authors the osteons position and diameters were chosen randomly based on hypersecant distribution curve until they fills 60% of an area with same dimensions as micrographs. Then, Dagum (4P) distribution curve was used to choose randomly the Haversian canal diameters until their total area lies in the range 1.6%-5.3%. Random positions, osteons and Haversian canal diameters were then used as an input to Abaqus 6.10 [22].

2.2 Mechanical Properties

In this study the material properties of osteonal cortical bone microstructural constituents and homogenised properties are experimentally measured. All the data was measured for fresh bovine diaphysis femora. Regarding the homogenised material properties, the data was based on experimental measurements by the authors [23]. Also, the elastic data of osteons and interstitial bone were measured using nanoindentation technique by the authors [24]. As shown by Lakes *et al.* [25] cement lines posses an isotropic viscoelastic behaviour due to their specific chemical composition. Therefore, its elastic properties differs from the osteons that they are encircled. In this study, the elastic properties of cement lines was taken 25% lower than that for osteons based on the multiple scale model by Budyn *et al.* [18]. Osteons, interstitial bone and cement lines were chosen to be isotropic in this model. The Poisson's ratio of the osteons, interstitial bone, cement lines and homogenised properties area were chosen based on literature data [18, 26]. **Table 1** summarises the elastic material properties for homogenized and microstructural constituents.

2.3 XFEM-Based Cohesive Behaviour and Fracture Properties

In this study, an XFEM-based cohesive segment for a crack propagation analysis has been used to simulate crack initiation and propagation for both homogeneous and microstructural models. The formulae and laws that govern the behaviour of this approach are similar to those used for cohesive elements using traction-separation constitutive behaviour. The similarity comes from the use of the linear elastic

traction-separation model, damage initiation criterion and damage evolution criterion [22]. The initial stage of traction-separation model assumes linear elastic behaviour followed by damage initiation and evolution. Both elastic stiffness and the traction-separation behaviour are sufficiently defined by attribute an elastic properties to the material in an enriched region. In this study and for all the models, all elements were chosen as an enriched region. On the other hand, damage modelling allows the simulation of the degradation and eventual failure of an enriched element [22]. The failure in many biological materials is described based on elastic-damage driven criterion [18]. Human cortical bone is governed by strain based criterion [27]. In these models, the onset of fracture is based on the critical maximum principal strain. A value of 0.4% was chosen to initiate the cracks in the homogenised material as well as all the microstructural constituents [28, 29]. In a similar model, it was shown that cracks can be initiated perpendicular to maximum principal stress direction, mode I in tension [18], therefore, an initial crack of length 100 μm has been placed at the middle upper and lower boundaries perpendicular to the loading tensile direction, see Fig. 1b and c. Once the initiation criterion is met, cracks start to grow obeying the damage evolution law that describes the rate at which the cohesive stiffness is degraded [22]. Evolution of damage in our models is defined based on the energy required for failure (fracture energy) after the initiation of damage. The stress intensity factor for the homogenised material is based on data from Nalla *et al.* [30], and those for osteons and interstitial bone were taken by guidance from [8]. A ratio, $K_m/K_{cl} = 2$ where K_m and K_{cl} are interstitial bone and cement line stress intensity factors, were utilized to obtain the cement line stress intensity factor based on [31]. Table 1 summarizes the fracture energies used for homogenised and microstructural constituents. Regarding the model's elements, 4-node bilinear plain strain quadrilateral, CPE4R, elements were used. The total number of elements was 13561 and the total number of nodes was 14100. It is the current limitations of XFEM using Abaqus 6.10 [22] to use first order solid continuum elements.

All the models have been distorted under deformation control condition. A 1% strain has been applied to the right hand side of the microstructure cell in x-direction, while the left hand side was kept in place by constraining it in x-direction and only the middle point in y-direction, see Fig. 1b and c.

3. Results and Discussion

Three different numerical models: homogeneous, two phase composite and three phase composite were developed to investigate the effect of microstructural features of osteonal cortical bone tissue, particularly cement lines, upon the global behaviour and crack propagation paths. Relating the results of different models can shed the light on the distinctions between their behaviours. The quasi-static analysis of these models showed an obvious dissimilarity between their global stress-strain behaviour, see Fig. 2. Although the elastic moduli for all the models were approximately the same, but when the crack initiated and started to propagate the behaviours have changed. The model with cement lines demanded the highest applied stress and

applied strain for the microcracks to start growing. While the homogeneous model required the lowest values, the model without cement lines decided to stay in between, see Table 2. The cement lines' model required 17.5% applied stress higher for the microcracks to start evolving, while the model without cement lines required 16.9%. However, the difference between the applied stresses for the latter and model with cement lines was only 0.6%. Although the criterion used for crack initiation was the same for all the models, however heterogeneity accompanied with different topologies resulted in different stresses and strains distributions that are in turn lead to different required applied stresses to advance the microcracks. Unlike models with micro-features, the global stress-strain behaviour of the homogeneous model started to soften gradually immediately after the microcrack started to evolve. These results are also supported by Fig. 3 that showed at the same level of deformation microcracks extended for longer distances compared to the other models. Also, there was a significant difference between the microcracks' total length of the homogenised model and the composite models at its fracture point. Comparing the model without cement lines to the others; its global stress-strain behaviour is higher. It was noticed that with no cement lines the osteons tend to transmit more deformation to the matrix, while when cement lines are included osteons remain confined and reveal more deformation. This can explain the more hardening accompanied with no cement lines' model. This was also reported in another simulations Budyn *et al.* [18]. The homogenised model had the lowest fracture stress and strain while the model without cement lines had the higher values, see Fig. 2 and Table 3. The behaviour of the model including cement lines was somewhere between the homogenised model and the model without cement lines. Its final condition was not a percolation of the cell but rather one of the microcracks was frozen at a void and the other was arrested by a cement line. In this model, due to the limitations of the XFEM, the upper crack was unable to propagate any further to show the final crack path along with its final global stress-strain behaviour, and the lower microcrack had no opportunity to propagate because it was in the cement line custody. The final condition and the fracture point of models with and without cement lines are shown in insets in Fig. 2. Obviously, as the cell was not fully damaged in the model with cement lines, so its global behaviour started to harden again after their microcracks were stopped; the remaining undamaged material between the two microcracks started to behave elastically. On the other hand, at the fracture point of the model with no cement lines, its behaviour softened before a cell failure. These results indicate the direct effect of the microstructural heterogeneity on the global behaviour of cortical bone tissue. The final condition of the model possesses cement lines is consistent with our experimental results at the medial-transversal direction [23]. The model without cement lines feature required 27.5% of applied stress and 21.5% of applied strain higher than the homogenised model to achieve a cell percolation. In another way to find out the distinctions between the models, the total microcrack propagation length was measured and the deformation was recorded at each time increment; the relationship between them is shown in Fig. 3. An obvious difference between the total crack lengths at the same

deformation level was observed between the models. In the homogenised material model the microcracks did not find any obstacles to propagate and meet midway in a normal path to the applied load. This was not the case for the other models. Both the microcracks of the two composite models were extending in the same fashion up to a deformation of 0.0035 mm; this also can be seen in Fig. 4. As cement line stopped the microcrack to go, the total length of microcracks unchanged as the deformation evolved. Therefore, this relationship highlights the role of the cement line to inhibit microcracks. Also, the cement lines played an important role and forced the upper microcrack to find its way between two osteons, while when the cement lines were dismissed the maximum principal stress distribution has changed resulting in a kinky way of the microcrack, see Fig. 5 and 6. The total length of the microcracks in turn was longer in the model with no cement lines than that of the model with cement lines. Moreover, in the former the microcracks have extended until a complete fracture of the cell has happened leading to provide us with a full behaviour of its total length versus the applied deformation, which was not the case for the latter.

The simulation results of the model with cement lines showed two different paths; the upper microcrack went straight away between two osteons and split the one a head until it approached and has been halted by its Haversian canal, see Fig. 4a. It was obvious here that the upper microcrack followed a path between the two osteons and was affected by them. This is consistent with a simulation results in [19]. On the other hand, the lower microcrack deviated towards an osteon and tried to split it, but its cement line arrested the microcrack. It is worth noticing that the length of the lower microcrack when it hit the cement line was 175 μm ; this is consistent with an experimental study investigated short microcracks and showed that for microcracks of intermediate length (100-300 μm) were deflected as they hit the cement lines [10]. At the final increment of simulation it was noticed that while the upper and the lower microcracks have been halted at a void and a cement line, respectively, see Fig. 4a, they have managed to split both the homogenised model and model with no cement lines into a half, see Fig. 4b. The final crack path for the homogenised model was exactly perpendicular all the way long between the upper and lower microcracks to the applied load. The effect of the cement lines is also noticed upon the maximum principal stress distributions; see Figs. 5 and 6, the presence or the absence of the cement lines gave a completely different distributions resulting in different microcrack paths through the cell. The microcracks always tried to find their way normal to the maximum principal stress. The microlevel stresses showed sudden changes over Haversian canal and cement lines regions that controlled the microcrack propagation.

Obviously, there is an effect of the cement lines on the crack paths according to our study along with two other similar studies [18, 19], however it was reported in an experimental study that when the crack plane is perpendicular to osteons axis, the underlying microstructure has a much stronger influence on the crack path [30]. In the later case, it was observed that crack initiation and initial crack growth does not follow a path normal to the maximum tensile stress, but rather in the osteons' direction. It was concluded in that study that the cement lines, which is the interface

separating osteons from interstitial bone can provide a weak path for the crack propagation [30].

As trauma associated with high-speed transportations, sports injuries, and industrial accidents often involved fracture of bones, so the next step in our research is to investigate the effect of the microstructure of the Haversian cortical bone on the crack growth trajectories and on the global behaviour under transient loading conditions.

4. Conclusions

Various finite-element models were developed and implemented to study the effect of cement lines upon microcracks growth trajectories and the global behaviour of osteonal cortical bone tissue. These parameters of a three phase composite model containing a cement lines were related to another two models: one was a two phase composite model with no cement lines and the other was a model with homogenised material. Based on the obtained results from numerical simulations the following conclusions can be formulated:

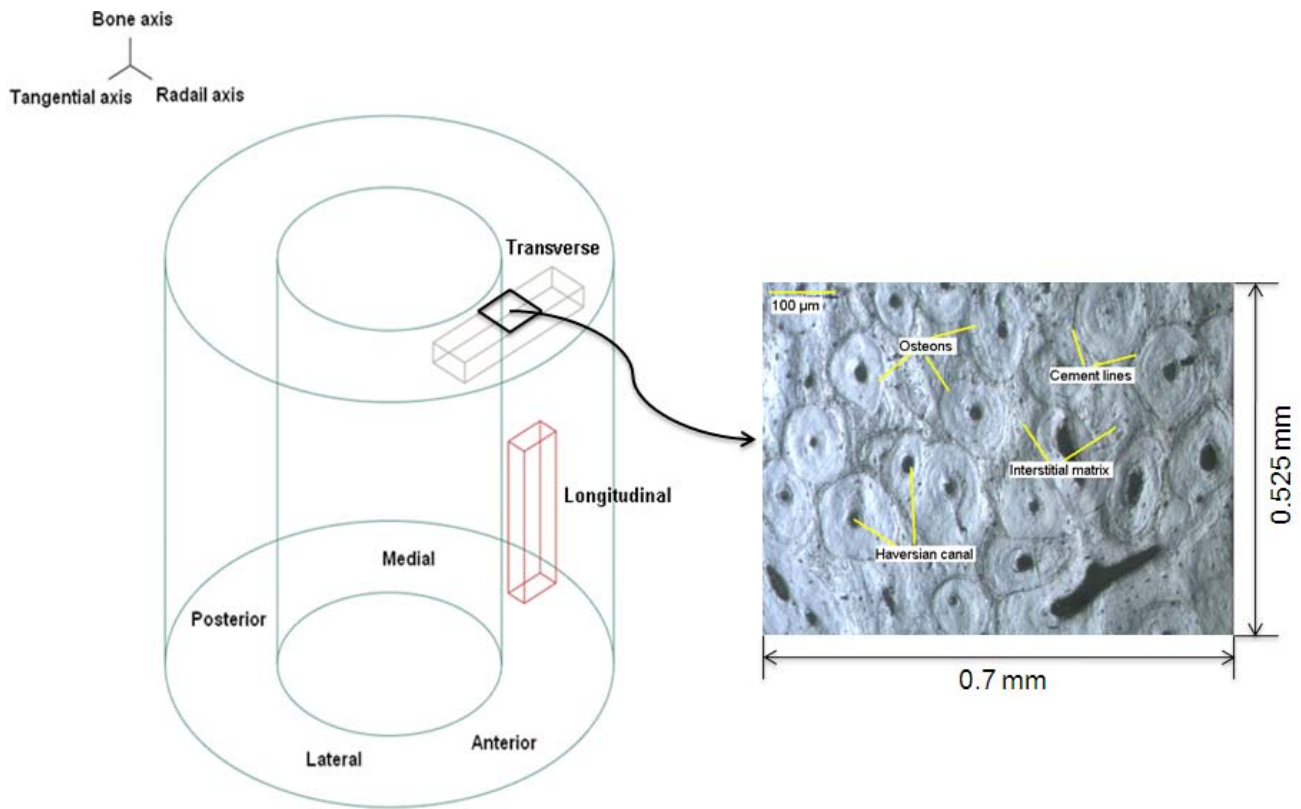
- Dissimilar global stress-strain behaviour was observed between the homogeneous material model and the composite material models.
- Implementing a cement lines demanded higher level of stress and strain to move microcracks.
- The homogeneous model started to soften immediately after the crack started to propagate, while the implementing a heterogeneous material model resulted in a hardening behaviour.
- A significant difference between the total microcrack length at the fracture point of the homogeneous model and the composite models was observed.
- The homogeneous model had the lowest final fracture stress and strain, the model without cement lines had the highest values, and the model with cement lines was halted at a point in between.
- The total microcrack length-deformation relationship highlights the role of the cement lines to inhibit the fracture at microscale level.
- The Haversian microstructure affects the maximum principal stress distribution that is in turn affect the microcracks propagation trajectories.

References

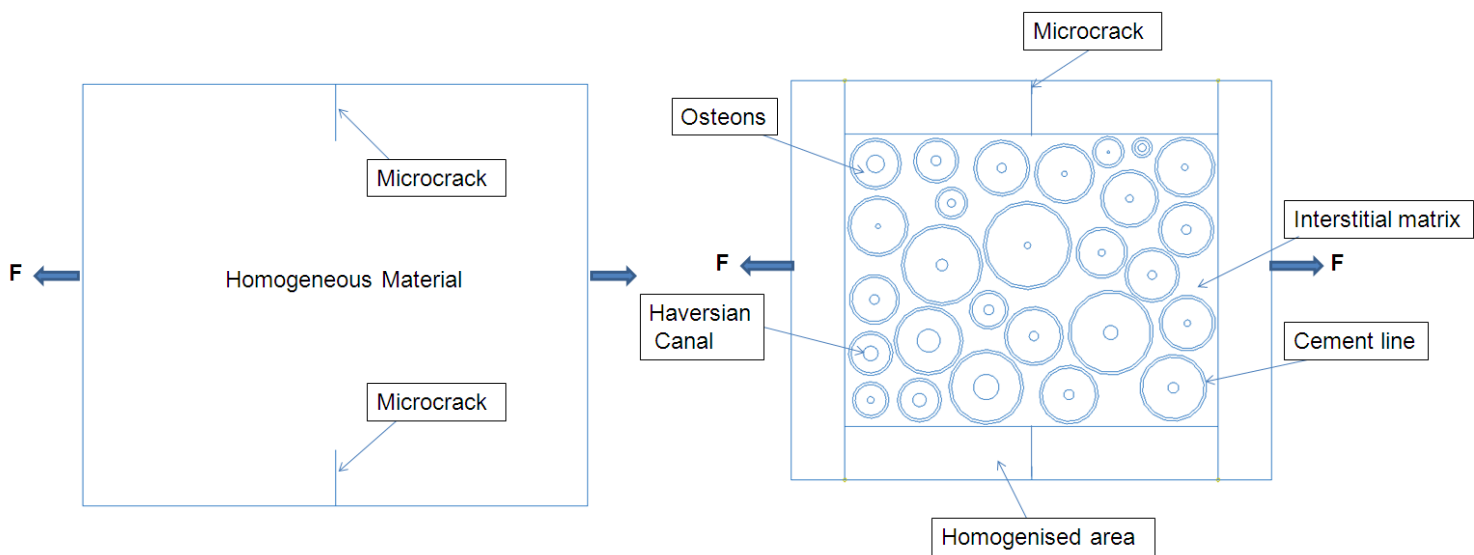
1. Ferriera, F., Vaz, M.A., Simoes, J.A., *Mechanical properties of bovine cortical bone at high strain rate*. Mater. Charact., 2006. **57**: p. 71-79.
2. Hogan, H.A., *Micromechanics modeling of Haversian cortical bone properties*. J. Biomech., 1992. **25**(5): p. 549-556.

3. Wang, X.D., Masilamani, N.S., Mabry, J.D., Alder, M.E., Agrawal, C.M., *Changes in the fracture toughness of bone may not be reflected in its mineral density, porosity and tensile properties*. Bone, 1998. **23**(1): p. 67-72.
4. Martin, R.B., Burr, D.B., *Structure, function and adaptation of compact bone* 1989, New York: Raven Press.
5. Bevill, G., Eswaran, S.K., Gupta, A., Papadopoulos, P., Keaveny, T.M., *Influence of bone volume fraction and architecture on computed large-deformation failure mechanisms in human trabecular bone*. Bone, 2006. **39**(6): p. 1218-1225.
6. Morgan, E.F., Bayraktar, H.H., Keaveny, T.M., *Trabecular bone modulus-density relationships depend on anatomic site*. J. Biomech., 2003. **36**(7): p. 897-904.
7. Guo, X.R., Liang, L.C., Goldstein, S.A., *Micromechanics of osteonal cortical bone fracture* J. Biomech. Eng., 1998. **120**: p. 112-117.
8. Mullins, L.P., sassi, V., McHugh, P.E., Bruzzi, M.S., *Differences in the crack resistance of interstitial, osteonal, and trabecular bone tissue*. Ann. Biomed. Eng., 2009. **37**(12): p. 2574-2582.
9. Zioupos, P., *Accumulation of in vivo fatigue microdamage and its relation to biomechanical properties in ageing human cortical bone*. J. Microsc. , 2001. **201**(2): p. 270-278.
10. Mohsin, S., O'Brien, F.J., Lee, T.C., *Osteonal crack barriers in ovine compact bone*. J. Ant., 2006. **208**: p. 81-89.
11. Boyce, H.M., Fyhire, D.P., Glotkowski, M.C., Radin, E.L., Schaffler, M.B., *Damage type and strain mode associations in human compact bone bending fatigue*. J. Orthop. Res., 1998. **16**: p. 322-329.
12. Martin, R., Yeh, O., Fyhire, D., *On sampling bone for microcracks*. Bone, 2007. **40**(4): p. 1159-1165.
13. O'Brien, F.J., Taylor, D., Lee, T.C., *Microcrack accumulation at different intervals during fatigue testing of compact bone*. J. Biomech., 2003. **36**(7): p. 973-980.
14. Atkinson, P.J., Hallsworth, A.S., *The spatial structure bone*, in *Progress in Anatomy*, R.J. Harrison, Navaratum, V., Editor. 1982, Cambridge University Press: Cambridge p. 179-199.
15. Mohsin, S., Taylor, D., Lee, T.C., *Three-dimensional reconstruction of Haversian system in ovine compact bone*. Eur. J. Morph., 2002. **40**: p. 309-315.
16. Prendergast, P.J., Huiskes, R., *Microdamage and osteocyte-lacuna strain in bone: a microstructural finite element analysis*. J. Biomech. Eng., 1996. **118**: p. 240-246.
17. Dong, X.N., Zhong, X.N., Huang, Y., Guo, X.E., *A generalized self-consistent estimate for the effective elastic moduli for fiber-reinforced composite materials with multiple transversely isotropic inclusions*. Int. J. Mech. Sci., 2005. **47**(6): p. 922-940.
18. Budyn, E., Hoc, T., *Multiple scale modeling for cortical bone fracture in tension using X-FEM*. REMN, 2007. **16**: p. 215-238.
19. Raeisi Najafi, A., Arshi, A.R., Eslami, M.R., Fariborz, S., Moeinzadeh, M.H., *Micromechanics fracture in osteonal cortical bone: A study of the interactions between microcrack propagation, microstructure and the material properties*. J. Biomech., 2007. **40**: p. 2788-2795.
20. Image-Pro Express, V., Version media cybernetics, 2005.

21. MATLAB7, V.R.a., *User's Manual, MATLAB, The MathWorks, UK, 2007.* 2007.
22. Abaqus, D.S.S.C., Providence, RI, USA, 2010. Theory manual -Version 6.10.
23. Abdel-Wahab, A.A., Alam, K., Silberschmidt, V.V., *Analysis of anisotropic viscoelastoplastic properties of cortical bone tissues.* Journal of the Mechanical Behavior of Biomedical Materials (2010), doi:10.1016/j.jmbbm.2010.10.001, 2010.
24. Abdel-Wahab, A.A., Maligno, A.R., Silberschmidt, V.V., *Micro-scale numerical model of bovine cortical bone: analysis of plasticity localization*, in *Biennial Conference on Engineering Systems Design and Analysis, ESDA2010*, 2010, ASME: Istanbul, Turkey.
25. Lakes, R., Saha, S., *Cement line motion in bone.* Nature, 1979. **204**: p. 501-503.
26. Sabelman, E.E., Koran, P., Diep, N., Lineaweaver, W.C., *Collagen/hyaluronic acid matrices for connective tissue repair* in *First Smith & Nephew international Symposium: Advances in Tissues Engineering and Biomaterials 1997*, 20-23 July.
27. Nalla, R.K., Stolken, J.S., Kinney, J.H., Ritchie, R.O., *Fracture in human cortical bone: local fracture criteria and toughening mechanisms.* J. Biomech., 2005. **38**: p. 1517-1525.
28. Bayraktar, H.H., Morgan, E.F., Niebur, G.L., Morris, G.E., Wong, E.K., Keaveny, T.M., *Compression of the elastic and yield properties of human femoral trabecular and cortical bone tissue.* J. Biomech., 2004. **37**: p. 27-35.
29. Pattin, C.A., Calet, W.E., Carter, D.R., *Cyclic mechanical property degradation during fatigue loading of cortical bone.* J. Biomech., 1996. **29**: p. 69-79.
30. Nalla, R.K., Kinney, J. H., Ritchie, R. O., *Mechanistic fracture criteria for the failure of human cortical bone.* Nature, 2003. **2**: p. 164-168.
31. Yeni, Y.N., Norman, T. L. *A formulation of the influence of osteons on the fracture toughness of cortical bone in the longitudinal crack growth*, 1999; Available from: <http://www.asbweb.org/conferences/1990s/1999/ACROBAT/024.PDF>.



(a)



(b)

(c)

Figure 1: (a) Light microscopy micrograph of transverse-radial cross-section of osteonal bovine cortical bone tissue, (b) schematic illustration of homogeneous model, and (c) schematic illustration of microstructural features models.

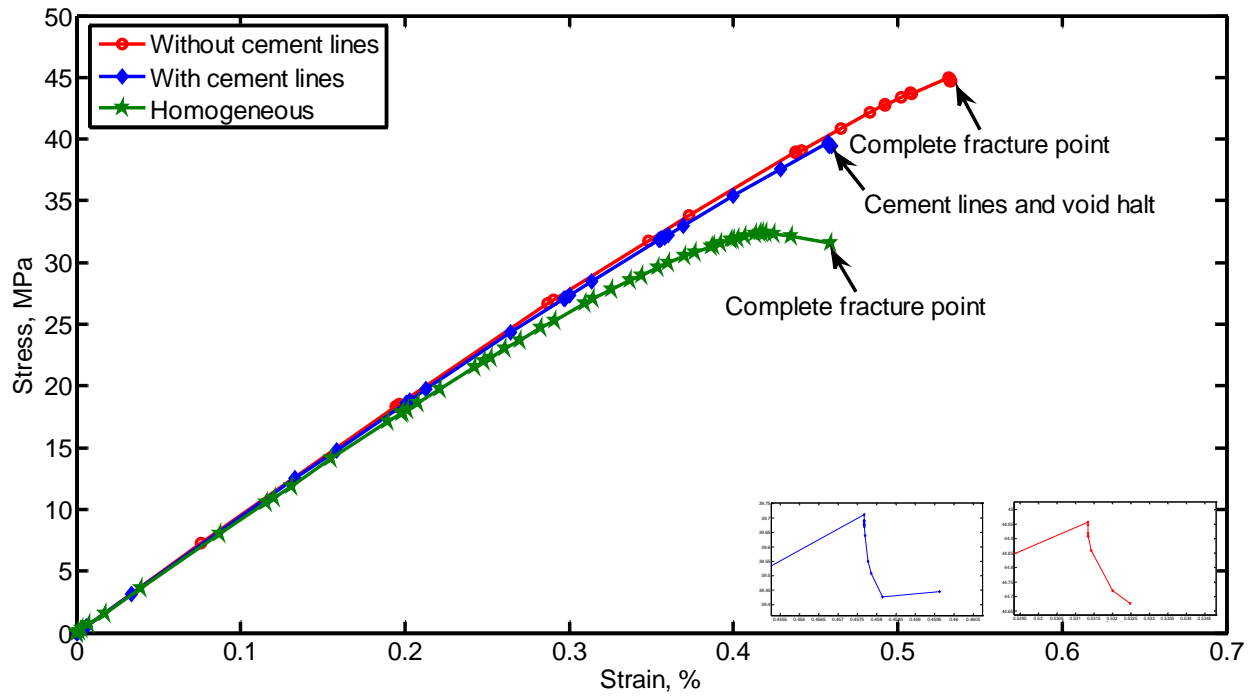


Figure 2: Stress strain behaviour of homogeneous, without cement lines and with cement lines models under tension

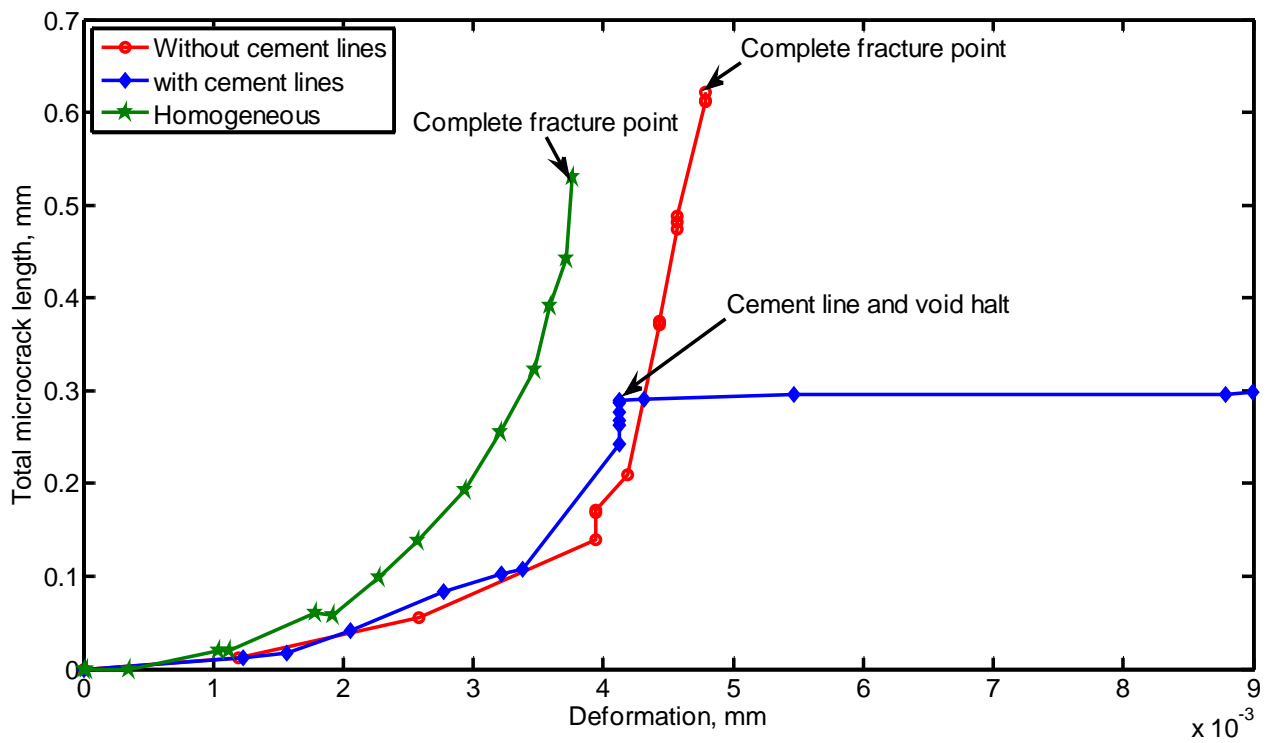
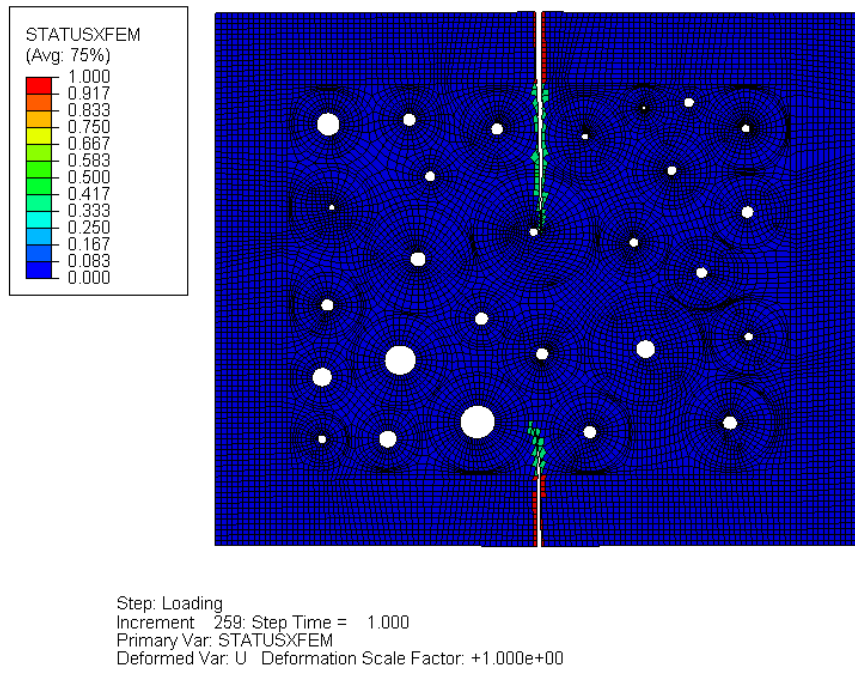
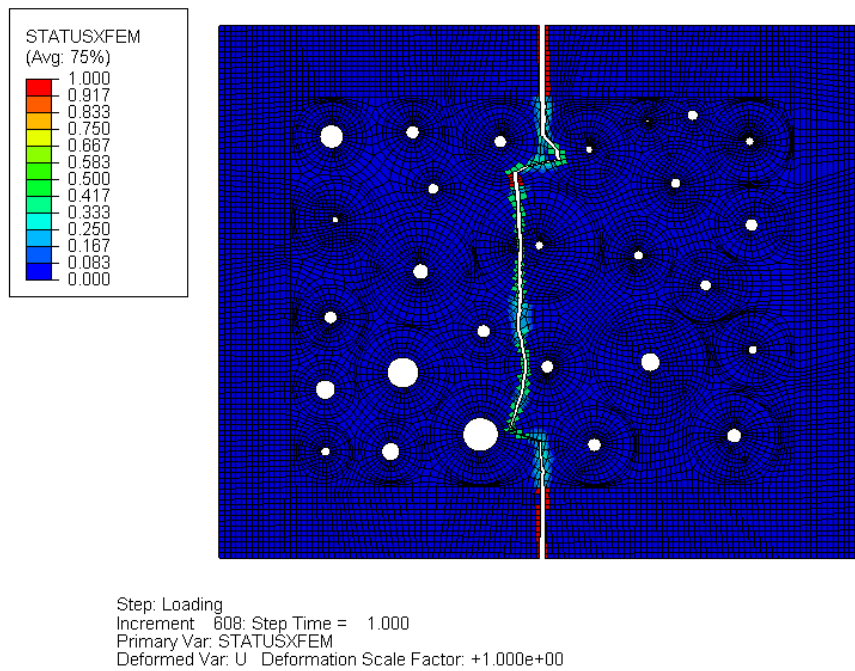


Figure 3: Total crack length versus deformation of homogeneous, without cement lines, and with cement lines models under tension



(a)



(b)

Figure 4: Final crack propagation paths for (a) with cement lines model and (b) without cement lines model of osteonal cortical bone tissue

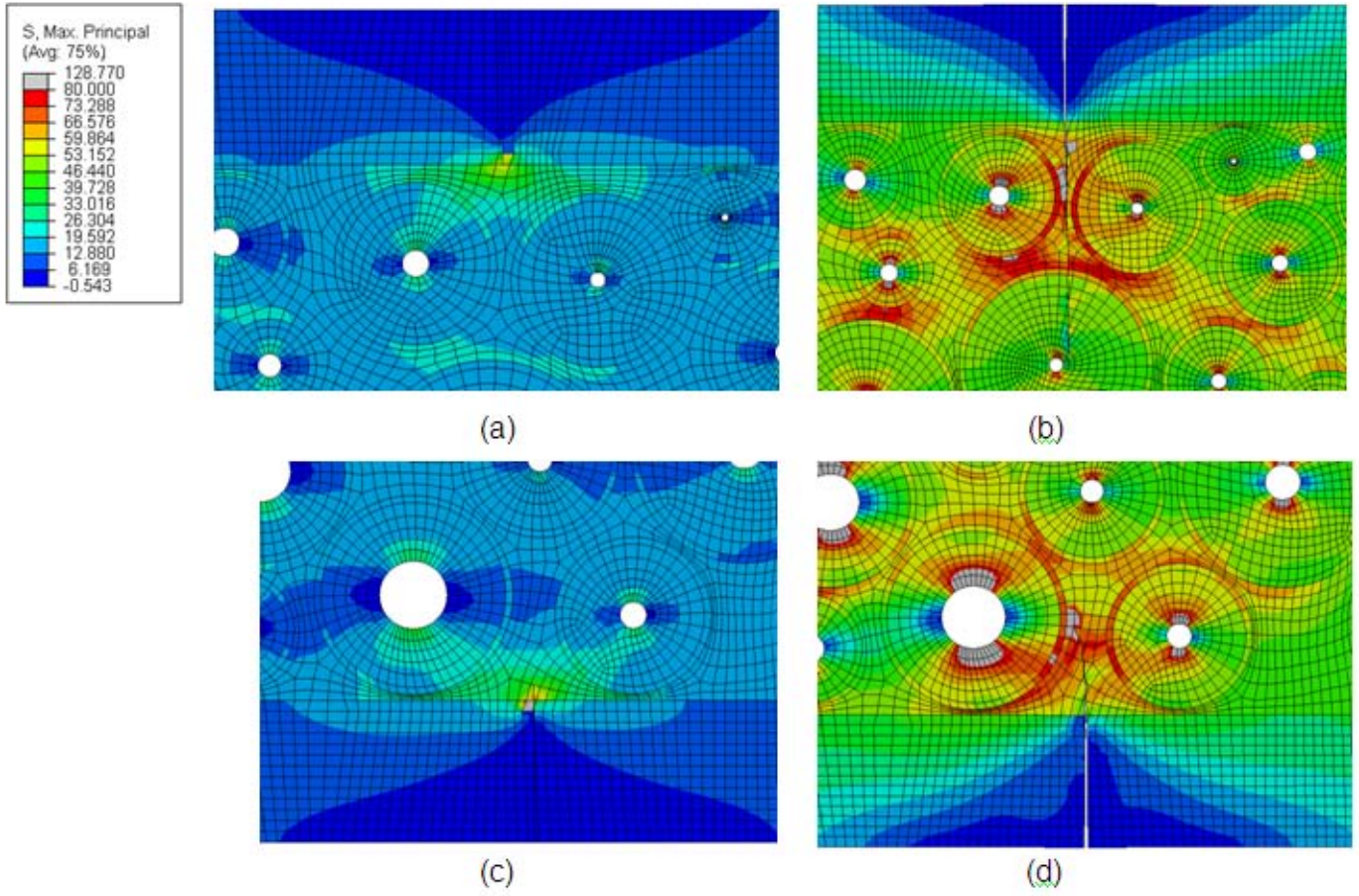


Figure 5: Maximum principal stress distributions around upper and lower microcrack, (a), (c) at crack initiation increment, and (b), (d) at cement line and void halt increment of with cement lines model for osteonal cortical bone tissue

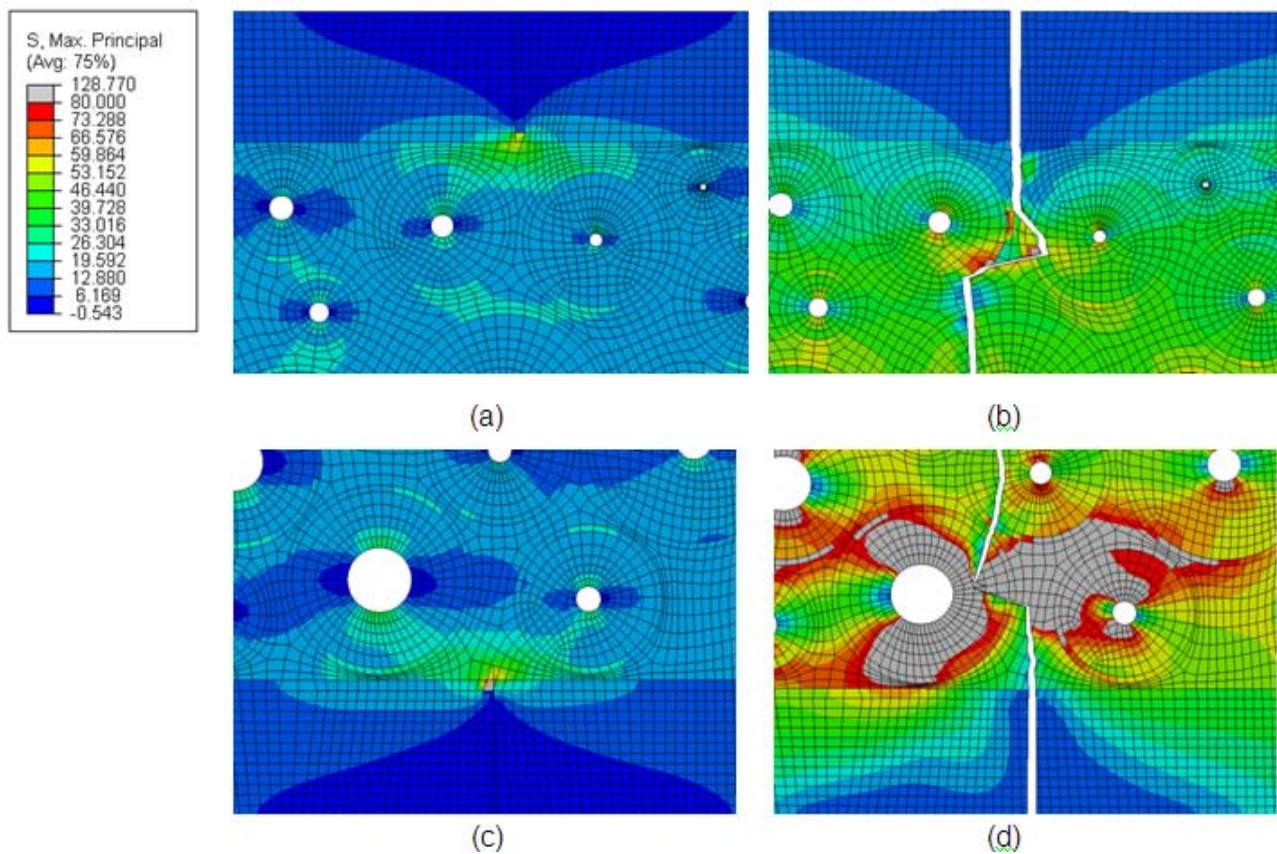


Figure 6: Maximum principal stress distributions around upper and lower microcrack, (a), (c) at crack initiation increment, and (b), (d) at cement line and void halt increment of without cement lines model for osteonal cortical bone tissue

Table 1: Elastic properties and strain energy release rate of microscopic features and homogenised material of osteonal cortical bone tissue in transverse direction

	Elastic modulus (GPa)	Poisson's ratio	Strain energy release rate N/mm
Homogenised material	10.46	0.167	0.422 [30]
Osteons	9.13	0.17 [18]	0.86
Interstitial matrix	14.122	0.153 [18]	0.238
Cement lines	6.85 [18]	0.49 [26]	0.146

Table 2: Crack initiation applied force, applied stress, applied strain and deformation of three different numerical models in tension

	Crack initiation conditions			
	Applied force (N)	Applied stress (MPa)	Applied strain (%)	Applied deformation (mm)
Homogeneous	2.38	10.60	0.115	0.0010
Without cement lines	2.87	12.77	0.133	0.0012
With cement lines	2.89	12.85	0.136	0.0013

Table 3: Complete fracture applied force, applied stress, applied strain and deformation of homogeneous and without cement lines models as well as cement lines and voids half for with cement lines model in tension

	Crack final conditions			
	Applied force (N)	Applied stress (MPa)	Applied strain (%)	Applied deformation (mm)
Homogeneous	7.29	32.42	0.418	0.0038
Without cement lines	10.06	44.69	0.533	0.0048
With cement lines	8.88	39.44	0.459	0.0041